Cell Biol Toxicol
https://doi.org/10.1007/s10565-022-09750-0

RESEARCH

CircJag1 promotes apoptosis of ethylene thiourea–exposed anorectal malformations through sponging miR-137-3p by regulating Sox9 and suppressing Wnt/β-catenin pathway during the hindgut development of rat embryos

Si Ying Li · Chen Yi Wang · Xiao Gao Wei · Xiao Bing Tang · Zheng Wei Yuan · Yu Zuo Bai

Received: 28 April 2022 / Accepted: 19 July 2022

Abstract Anorectal malformations (ARMs) are common birth defects involving congenital structural anomalies of the gastrointestinal tract. As an important component of non-coding RNAs, circular RNAs (circRNAs) widely participate in the digestive system development; however, the specific molecular mechanism of their involvement in ARM occurrence remains obscure. Herein, we generated rat models of ARMs induced by ethylene thiourea. A novel circRNA (circJag1) was screened and identified by RNA-Seq, which is remarkably upregulated in hindgut tissues of ARM rat embryos. In vivo experiments, colocation analysis via fluorescence in situ hybridization, and immunofluorescence further demonstrated that the disordered circJag1/miR-137-3p/Sox9 expression caused a spatiotemporal imbalance in the urorectal septum (URS) of ARMs. In vitro, functional assays confirmed that circJag1 upregulation resulted in the degradation of nuclear β-catenin, C-myc, and Cyclin D1 in rat intestinal epithelial cells, as well as the promotion of apoptosis and suppression of cell proliferation. Mechanistically, dual-luciferase reporter assay and RNA immunoprecipitation assay indicated that circJag1 acted as a miR-137-3p sponge, thereby inhibiting its repressive effect on its target Sox9. Further experiments showed that a loss of Sox9 abolished the circJag1-mediated increase in apoptosis. In conclusion, aberrantly high circJag1 expression promotes epithelial apoptosis by suppressing the canonical Wnt/β-catenin pathway via the miR-137-3p/Sox9 axis, which leads to fusion failure of the URS and cloacal membrane, and eventually contributed to ARMs. Our achievements might boost the comprehension of ARM pathogenesis and could provide a novel candidate target for the development of therapies for ARMs to complement surgical treatment.

Supplementary Information The online version contains supplementary material available at https://doi.org/10.1007/s10565-022-09750-0.

S. Y. Li · C. Y. Wang · X. G. Wei · X. B. Tang · Y. Z. Bai (✉)
Department of Pediatric Surgery, Shengjing Hospital of China Medical University, No. 36 Sanhao Street, Heping District, Shenyang 110004, Liaoning, China
e-mail: baiyz1216@126.com

Z. W. Yuan
Key Laboratory of Health Ministry for Congenital Malformation, Shengjing Hospital of China Medical University, No. 36 Sanhao Street, Heping District, Shenyang 110004, Liaoning, China

Highlights

- CircJag1 was remarkably upregulated in ARM hindgut tissues during rat embryo development.
- CircJag1 acts as a competing endogenous RNA to sequester miR-137-3p, resulting in activation of miR-137-3p-target Sox9, and then promote degradation of β-catenin and turn off Wnt pathway.
- Abnormal expression of circjag1 may result in fusion failure of URS and CM by reducing epithelial proliferation and promoting apoptosis.

Published online: 05 August 2022

Keywords Anorectal malformations · Apoptosis · Circular RNA · CircJag1 · Wnt/β-catenin pathway

Introduction

Anorectal malformations (ARMs) have a broad spectrum of clinical phenotypes, such as stenotic anus, rectourethral fistula, rectal vestibular fistula, and anal atresia, which makes ARMs are common congenital structural anomalies, and prevalence rates of approximately 1/5000 live births (Falcone et al. 2007; Kluth 2010; Wood and Levitt 2018). Because the contours of the distal rectum and anus are difficult to clearly show through imaging, ARMs are hard to diagnose in the prenatal period. Although the anatomical anomalies can be corrected by delicate surgical reconstructive surgery, many patients experience postoperative defecation dysfunction, and these complications substantially disrupt their quality of life (Bai et al. 2000; Grano et al. 2013). Therefore, elucidating the fundamental molecular mechanisms of ARMs is of great significance for the development of novel early diagnosis and effective treatments.

Owing to the difficulty in obtaining human embryos with ARMs, ethylene thiourea (ETU) is the most common method for establishing rat embryonic ARM models which can be used to study interventions and the pathogenesis of ARMs conveniently (Macedo et al. 2007; Qi et al. 2002). Typical phenotypes of the ETU-induced ARM rat model are similar to those of neonates with ARMs; thus, many scholars have used this model to study dynamic morphological variation and molecular mechanisms underlying ARMs (Mandhan et al. 2006; Tang et al. 2014). During normal cloacal development, the downward extension of the urorectal septum (URS) completely separates the rectum from the urethra and bladder (Bai et al. 2004; Qi et al. 2000a). Dynamic observations and molecular analyses of ARMs induced by ETU in rats have suggested that, excessive endodermal epithelial apoptosis can lead to the fusion between the URS and cloacal membrane (CM) fall through, which may be an important reason of ARMs (Qi et al. 2000b; Sasaki et al. 2004). Consequently, further studies of the exact molecular mechanism linking apoptosis and ARMs are urgently needed.

ARMs caused by both hereditary and environmental factors according to epidemiological and animal experiments (Khanna et al. 2018; Wijers et al. 2014; Wang et al. 2015). Our research group has mainly focused on mRNA expression profiles during rat embryonic hindgut development (Li et al. 2021a; Tang et al. 2014). With the iterative refinement of sequencing technology, functions of circular RNAs (circRNAs) have been revealed in various biological processes during the development of embryos. Furthermore, circRNAs widely participate in the digestive system development. CircRNAs are characterized as covalent, closed-loop structures without 5′–3′ polarity or a poly-A tail (Lasda and Parker 2014). The special construction naturally protects circRNAs from degradation by RNA exonucleases, RNA enzyme R, and debranching enzymes. The stability and tissue specificity of circRNAs make them promising diagnostic biomarkers for diseases (Zhou et al. 2018, 2022). Functionally, mounting evidence have proven that circRNAs act as sponges for microRNAs (miRNAs) to modulate the repression of the target mRNA (Misir et al. 2022). However, the roles of circRNAs in anorectal development and particularly in ARMs were rarely understood.

SRY-related (SOX) transcription factor family members, which encode transcription factors with a high mobility group (HMG)–type DNA-binding domain, are extensively involved in ontogenesis and determine cell destiny and identity in many lineages (Schepers et al. 2002). Sox gene mutations are associated with congenital disorders and could result in developmental defects and syndromes, including severe defects, such as skeletal dysmorphism, cardiovascular anomalies, and sex reversal (Kamachi and Kondoh 2013). Liu et al. found that the expression levels of *Sox10* in colon samples from patients with Hirschsprung's disease and intestinal neurodysplasia are significantly higher than levels in normal controls (Liu et al. 2019). Shi et al. proved that *Sox9* can inhibit the proliferation of intestinal epithelial cells in mice (Shi et al. 2013). Recently, the important roles of the *Sox9* gene in early embryonic development have been reported (Chatzeli et al. 2017; Song and Park 2020). Moreover, *Sox9* could inhibit Wnt/β-catenin signaling activity in the developing intestinal epithelium (Akiyama et al. 2004; Bastide et al. 2007; Formeister et al. 2009; Topol et al. 2009). Numerous studies have shown that the wingless-type MMTV integration site family (Wnt) signaling pathway is critical in hindgut development (Kim et al. 2007; Miyagawa et al. 2014;

Ng et al. 2014; Khanna et al. 2018). β-Catenin plays an important role in regulation of cell differentiation and morphogenesis during embryogenesis, which is also a critical component of canonical Wnt signaling (Haegel et al. 1995). Topol et al. confirmed that Sox9 could promote β-catenin phosphorylation in the nucleus and its subsequent degradation in chondrocytes (Topol et al. 2009). Hence, we speculated that Sox9 may play a vital function in hindgut development via the Wnt/β-catenin signaling pathway.

In our previous study (Li et al. 2021b), we performed high-throughput sequencing of hindgut tissues of rat embryos with or without ETU-induced ARMs and found that circJag1 (novel_circ_011174 from RNA-sequencing; circular jagged canonical Notch ligand 1; derived from exons 3 and 6 of *Jag1*) was upregulated obviously in the ARM group compared to in the normal group. In the current study, we determined the differences in spatiotemporal expression of circJag1 during hindgut development between normal rat embryos and rat embryos with ARMs from gestational day (GD) 14 to GD16, the key time period for anorectal development. We further clarified the role of circJag1 in ARMs and its potential underlying mechanisms. Additionally, for the first time in this study, we explored the relationship between the circJag1/miR-137-3p/Sox9 axis and Wnt/β-catenin signaling pathway. Our observations may shed light on a novel pathophysiologic mechanism and serve as a useful foundation for the progress of preventive and treatment strategies for ARMs.

Materials and methods

RNA-Seq and bioinformatics analysis

Specific methods of RNA-Seq have been described in our previous studies (Li et al. 2021b). The datasets used in this study have been uploaded to the Gene Expression Omnibus database (GSE159306). In comparisons between groups, it was revealed that circRNAs with $|FC| \geq 2$ and $p < 0.05$ are differentially expressed. The statistical analysis was accomplished by R software (version 3.6.3; R Foundation for Statistical Computing, Vienna, Austria). The heat map and Venn diagram are visualized using GGploT2 and GGdendro.

Ethics statement

Ethics approval for the study was obtained from the Ethics Committee of our institution (2020PS357K). All of the animal experiments were strictly conducted according to the guidelines for the care and use of laboratory animals.

Animal and tissue preparation

The detailed process for the collection of anorectal tissues from ARM and normal rat embryos was followed by the previous study (Tang et al. 2014). In the aggregation, 60 pregnant Wistar rats (7–9 weeks, 250–280 g) were prepared. Half of the rats were gavaged by 1% ETU (Sigma-Aldrich; Merck Millipore, Darmstadt, Germany) on GD10 in accordance with125 mg/kg, whereas the remainder of the rats received an equivalent amount of normal saline as a control. Rodents were reared in a SPF (specific pathogen-free) environment, which room temperature was maintain in 22 ± 2°C, humidity was maintain in 55 ± 5%, light/dark cycle per 12 h, and available water and food for free.

There were 341 ARM embryos with short tails or no tails that were induced by ETU, as determined by light microscopy (OLYMPUS CX22; Tokyo, Japan), and 420 normal embryos treated by saline were obtained by cesarean section on GD14, GD15, and GD16. There are 84.8% (341/402) rat embryos in the ETU-treated group where ARMs occurred after excluding 21 that died in utero. A total of 430 embryos were formalin-fixed and paraffin-embedded, and then, the 4-μm-thick serial sections in sagittal view were used for fluorescence in situ hybridization (FISH), immunohistochemistry (IHC), and immunofluorescence (IF). Other samples were immediately frozen in liquid nitrogen for further quantitative real-time polymerase chain reaction (qRT-PCR) and Western blotting.

Terminal deoxynucleotidyl transferase dUTP nick end labeling (TUNEL)

Sections were deparaffinized with xylene and hydrated with an alcohol gradient. After transfection on glass slides in a 6-well plate, 4% formaldehyde was used to fix the cells. Following the instructions provided with the TUNEL Kit (Roche, Basel, Switzerland),

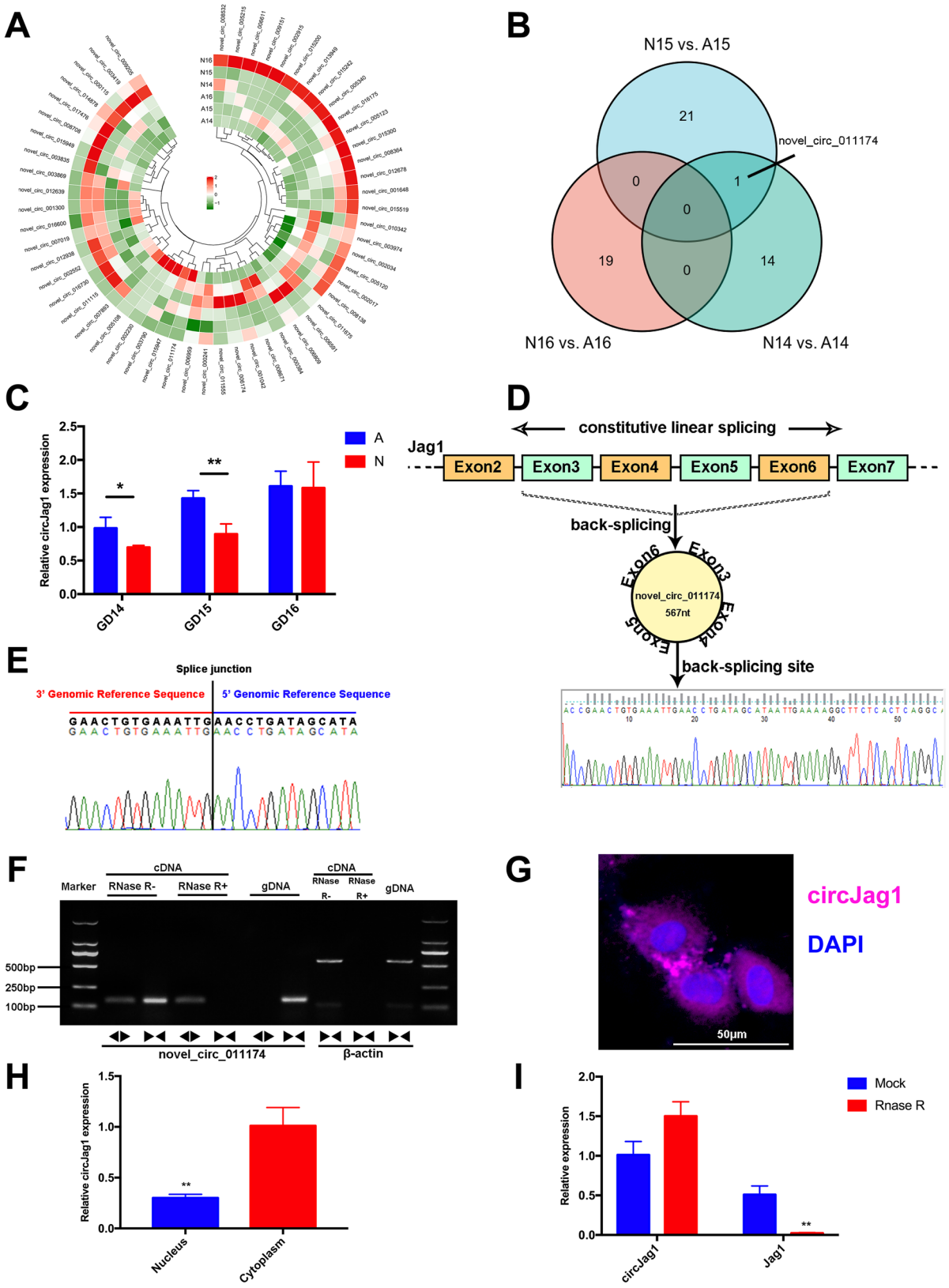
A
B
N15 vs. A15
21
novel_circ_011174
0
1
0
19
0
14
N16 vs. A16
N14 vs. A14
C
Relative circJag1 expression
A
N
*
**
GD14
GD15
GD16
D
constitutive linear splicing
Jag1
Exon2
Exon3
Exon4
Exon5
Exon6
Exon7
back-splicing
novel_circ_011174
567nt
back-splicing site
E
Splice junction
3' Genomic Reference Sequence
5' Genomic Reference Sequence
GAACTGTGAAATTGAACCTGATAGCATA
F
Marker
cDNA
RNase R-
RNase R+
gDNA
cDNA
RNase R-
RNase R+
gDNA
500bp
250bp
100bp
novel_circ_011174
β-actin
G
circJag1
DAPI
50μm
H
Relative circJag1 expression
**
Nucleus
Cytoplasm
I
Mock
Rnase R
Relative expression
**
circJag1
Jag1

◂**Fig. 1** CircJag1 expression pattern in rat intestinal epithelial cells. **A** Heat map of 55 differentially expressed circRNAs between hindgut tissues in normal and ETU-induced ARMs. Each group represents a mean of three biological replicates. **B** Venn diagram showing the overlap among the 55 differentially expressed circRNAs between the three time points; only novel_circ_011174 (circJag1) was identified at both GD14 and GD15. **C** Validation of circJag1 by qRT-PCR in normal and ARM hindgut samples. Six independent experiments were performed in triplicate. β-Actin was used as an internal control. **D** Schematic illustration showing Jag1 exons 3 to 6 circularization to form circJag1. **E** The sequence of circJag1 in RNA-Seq consistent with the result of Sanger sequencing. **F** The presence of circJag1 was validated in IEC-6 by PCR followed by agarose gel. Divergent primers amplified circJag1 from cDNA with or without RNase R, but not from gDNA. β-Actin was used as a negative control. **G** Representative FISH images of IEC-6 stained with circJag1 were shown. **H** qRT-PCR showed that circJag1 mainly expressed in the cytoplasm of IEC-6. The amount of circJag1 was normalized to the value measured in the cytoplasm. **I** Total RNAs of IEC-6 were digested with or without RNase R followed by qRT-PCR detection of circJag1 and Jag1 expression. Jag1 was detected as the RNase R-sensitive control. $^{*}p < 0.05$; $^{**}p < 0.01$. N, normal group; A, ARM group; GD, gestational day

the reaction mixture was prepared for samples incubated for 2h at 37 °C. Images were obtained under an Eclipse 80i microscope (Nikon, Tokyo, Japan). The average number of positive cells was divided by the total number of cells to calculate the apoptosis rate.

IF

After transfection on glass slides in 6-well plates, the cells were treated with 4% formaldehyde for 15 min and 10% goat serum (Biological Industries, Beit HaEmek, Israel) for 30 min. Then, the primary anti-β-catenin (1:100; Proteintech) was used to incubate with the cells at 4 °C continued for 16 h. The secondary antibody Alexa Fluor 594-conjugated (1:200; Proteintech) were used to incubate with IECs at room temperature continued for 1 h. Eclipse 80i microscope (Nikon, Tokyo, Japan) was used to obtain the images. Fluorescence signals and nuclear-plasma ratio were quantified by ImageJ. The quantitative methods reference studies that have been reported in the literature (Anguissola et al. 2011). In brief, the gray value of the entire cell and the cell nucleus was measured by ImageJ, and the nuclear-plasma ratio = the gray value of the cell nucleus/(the gray value of the entirety cell − the gray value of the cell nucleus). The nuclear-plasma ratio of each group was from the cell of three separate experiments, each nuclear-plasma ratio of individual experiment was the average of three field which selected randomly under microscope, and each nuclear-plasma ratio of the field was the average of three cell selected randomly in it.

IHC

Sections were deparaffinized and hydrated according to the common practice. Three percent H_2O_2 was used to incubate with the sections for 15 min in order to block the endogenous peroxidase activity. After antigen retrieval by sodium citrate, 10% goat serum (Thermo Fisher Scientific) was used to incubate the sections for 30 min to reduce false positives. Then, the primary antibody (anti-Sox9, 1:100 dilution; Abcam, ab185230) was used to incubate with the sections at 4 °C continued for 16 h, and then incubated with a horseradish peroxidase-conjugated secondary antibody (Thermo Fisher Scientific) at room temperature for 30 min. The 3,3′-diaminobenzidine (DAB; Sigma) was used to visualize the immunoreactivity, and the nuclei were stained with hematoxylin. Tissue sections were checked under a microscope (NIKON CE1 Confocal Microscope). The image processing was accomplished by Adobe Photoshop. ImageJ was used for quantitative analysis.

Statistical analysis

Statistical analyses were performed using SPSS 13.0 (IBM Corporation, Armonk, NY, USA). All data were obtained from at least three independent experiments performed in triplicate, and the results are presented as mean ± standard deviation (SD). Statistically significant differences between groups were identified by Student's *t*-tests (two-group comparison). One-way analysis of variance followed by Tukey's post-hoc analysis (multigroup comparison) was used to examine the difference as appropriate. Values of $p < 0.05$ were considered significant.

Results

CircJag1 is expressed in rat intestinal epithelial cells

Based on our previously generated high-throughput sequencing data, 55 significantly differentially expressed circRNAs filtered by $|FC| \geq 2$ and $p < 0.05$ from hindgut tissues of rat embryos with and

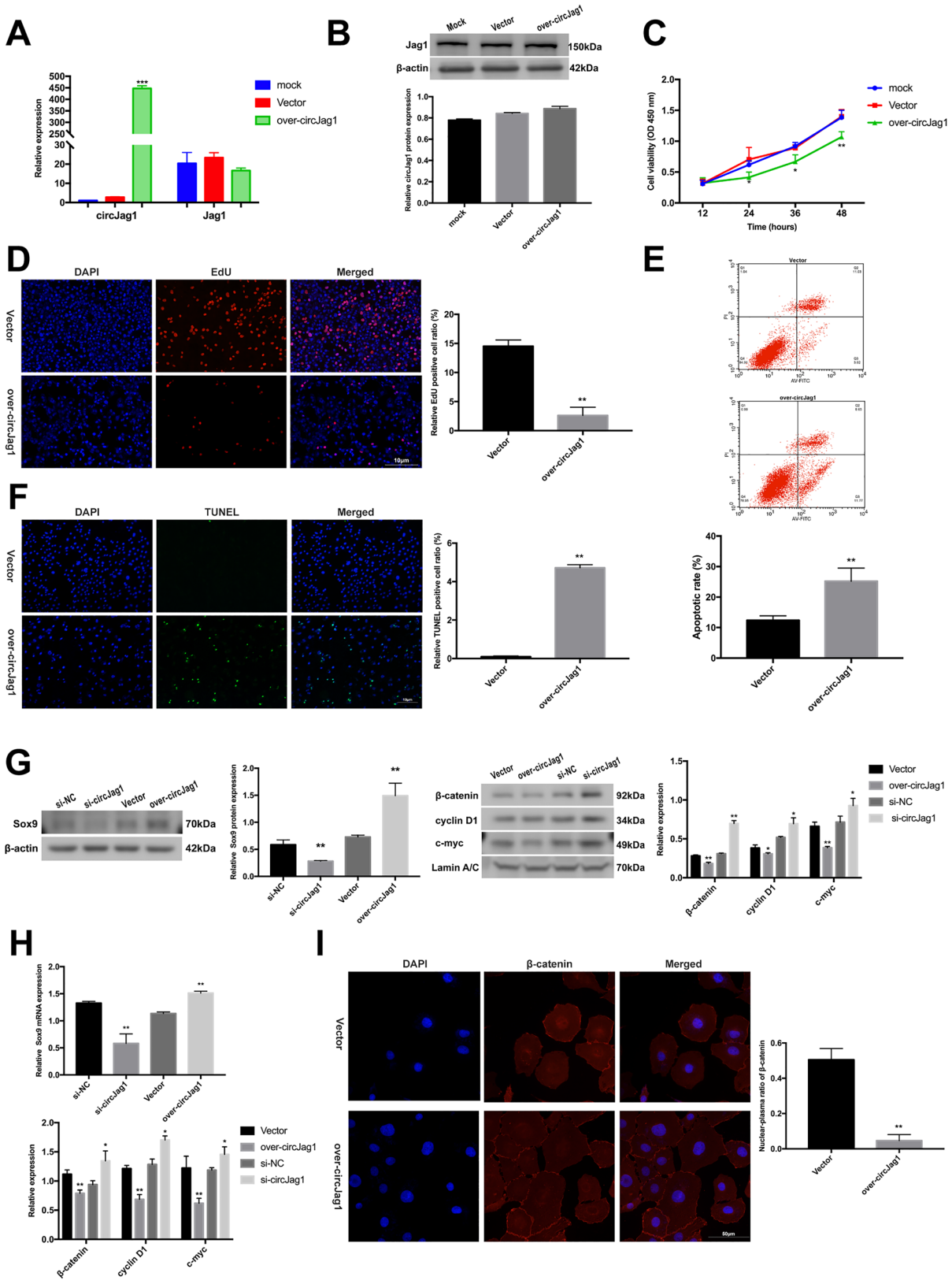
A
Relative expression
mock
Vector
over-circJag1
circJag1
Jag1
B
Mock
Vector
over-circJag1
Jag1
150kDa
β-actin
42kDa
Relative circJag1 protein expression
C
Cell viability (OD 450 nm)
Time (hours)
D
DAPI
EdU
Merged
Vector
over-circJag1
Relative EdU positive cell ratio (%)
E
Apoptotic rate (%)
F
TUNEL
Relative TUNEL positive cell ratio (%)
G
Sox9
70kDa
β-actin
42kDa
Relative Sox9 protein expression
β-catenin
92kDa
cyclin D1
34kDa
c-myc
49kDa
Lamin A/C
70kDa
si-NC
si-circJag1
H
Relative Sox9 mRNA expression
I
Nuclear-plasma ratio of β-catenin

◂**Fig. 2** CircJag1 promotes apoptosis and inhibits proliferation of rat intestinal epithelial cells. **A** qRT-PCR was used to detect the relative expression levels of circJag1 and Jag1 after transfection over-circJag1/vector in IEC-6. β-Actin was used as an internal control. **B** Western blotting was used to detect the protein expression levels of Jag1 after transfection over-circJag1/vector in IEC-6. **C, D** CCK-8 and EdU assays were used to detect the viability of IEC-6 after transfection over-circJag1/vector. **E, F** Flow cytometry with FITC-Annexin V/PI gating and TUNEL were used to detect apoptosis in IEC-6 after transfection over-circJag1/vector. Q2 and Q3 represent the percentage of late and early apoptotic cells in quadrants, respectively. **G** Protein expression levels of Sox9 in total protein and β-catenin, Cyclin D1, and C-myc in nuclear protein after transfection si-circJag1/si-NC/over-circJag1/vector. **H** Relative expression levels of Sox9 in total RNA and β-catenin, Cyclin D1, and C-myc in nuclear RNA after transfection si-circJag1/si-NC/over-circJag1/vector. Total RNAs were normalized to β-actin while nuclear RNAs were normalized to U6. **I** Immunofluorescence was used to detect the effect on β-catenin expression after transfection over-circJag1/vector in IEC-6. $*p < 0.05$; $**p < 0.01$

without ETU-treated were identified (Fig. 1A). Only novel_circ_011174 was identified at both GD14 and GD15, as shown in a Venn diagram (Fig. 1B). Accordingly, novel_circ_011174 was selected as the research object. We designed head-to-tail divergent primers for novel_circ_011174 (567nt circJag1) to validate the circRNA sequencing data in tissue samples by qRT-PCR. Compared to normal group, circJag1 was significantly upregulated in ARM group (Fig. 1C). Moreover, the amplified product of circJag1 was detected by Sanger sequencing, which confirmed that circJag1 was generated from exons 3 to 6 of *Jag1* (Fig. 1D, E). The cDNA and gDNA extracted from IEC-6 were amplified with convergent primers and divergent primers for circJag1, respectively. The divergent primers could amplify circJag1 in cDNA; however, they could not detect circJag1 in gDNA in IEC-6 (Fig. 1F). FISH showed that circJag1 is mainly expressed in the cytoplasmic fraction of IEC-6 (Fig. 1G), which was also confirmed by qRT-PCR (Fig. 1H). CircJag1 was indigestible by exonuclease ribonuclease R (RNase R), and a large amount of circJag1 expression can be detected after RNase R treatment, while linear *Jag1* mRNA was almost undetectable (Fig. 1I).

CircJag1 inhibits proliferation and promotes apoptosis

CircJag1 overexpression made no difference to Jag1 mRNA and protein levels (Fig. 2A, B); nevertheless, it reduced the proliferation rate of IEC-6 cells, as determined by CCK-8 and EdU assays (Fig. 2C, D). Flow cytometry and TUNEL assays also showed that circJag1 overexpression promoted apoptosis of IEC-6 cells (Fig. 2E, F). In cells transfected with three circJag1 si-RNAs, the si-1 knockdown efficiency was the highest at 68%; therefore, it was used in subsequent experiments (Fig. S1A). Moreover, we found that circJag1 high expression induced Sox9 expression, with concomitant reductions of β-catenin, C-myc, and Cyclin D1 levels through both Western blotting and qRT-PCR experiments (Fig. 2G, H). Accordingly, cellular immunofluorescence also showed that circJag1 overexpression resulted in reduced nuclear β-catenin levels (Fig. 2I). The results indicate that circJag1 overexpression enhances apoptosis and inhibits proliferation in IECs through Wnt/β-catenin pathway.

CircJag1 acts as sponge for miR-137-3p

Since circJag1 was highly expressed in the cytoplasm (Fig. 1G), we attempted to evaluate whether it could be a miRNA sponge to influence on gene expression. Argonaute RNA-induced silencing complex catalytic component 2 (Ago2) is a center member of the RNA-induced silencing complex (RISC), which binds to miRNA to target RNAs. RIP assays demonstrated that circJag1 was explicitly gathered in the immunoprecipitation of Ago2 pull down; however, circJag1 could not be detected in the control IgG (Fig. 3A). Two candidate miRNAs (miR-137-3p and miR-873-5p) were identified by intersection the predicted miRNA recognition elements in circJag1 sequence through miREAP, miRanda, and TargetScan. We used dual luciferase reporter assays to determine whether miR-137-3p and miR-873-5p regulates circJag1. Finally, only miR-137-3p mimics could significantly reduce the activity of LUC-circJag1 WT, whereas miR-137-3p mimics did not influence the activity of LUC-circJag1 MUT in 293T HEK cells (Figs. 3B and S1D). FISH showed the colocalization of circJag1 and miR-137-3p and Manders' overlap coefficient was 0.92 (Fig. 3C). The cytofluorogram is shown in Fig. S1C. We further confirmed the regulatory interaction between circJag1 and miR-137-3p. The overexpression of circJag1 significantly decreased miR-137-3p expression, and circJag1 silencing increased miR-137-3p expression (Fig. 3D).

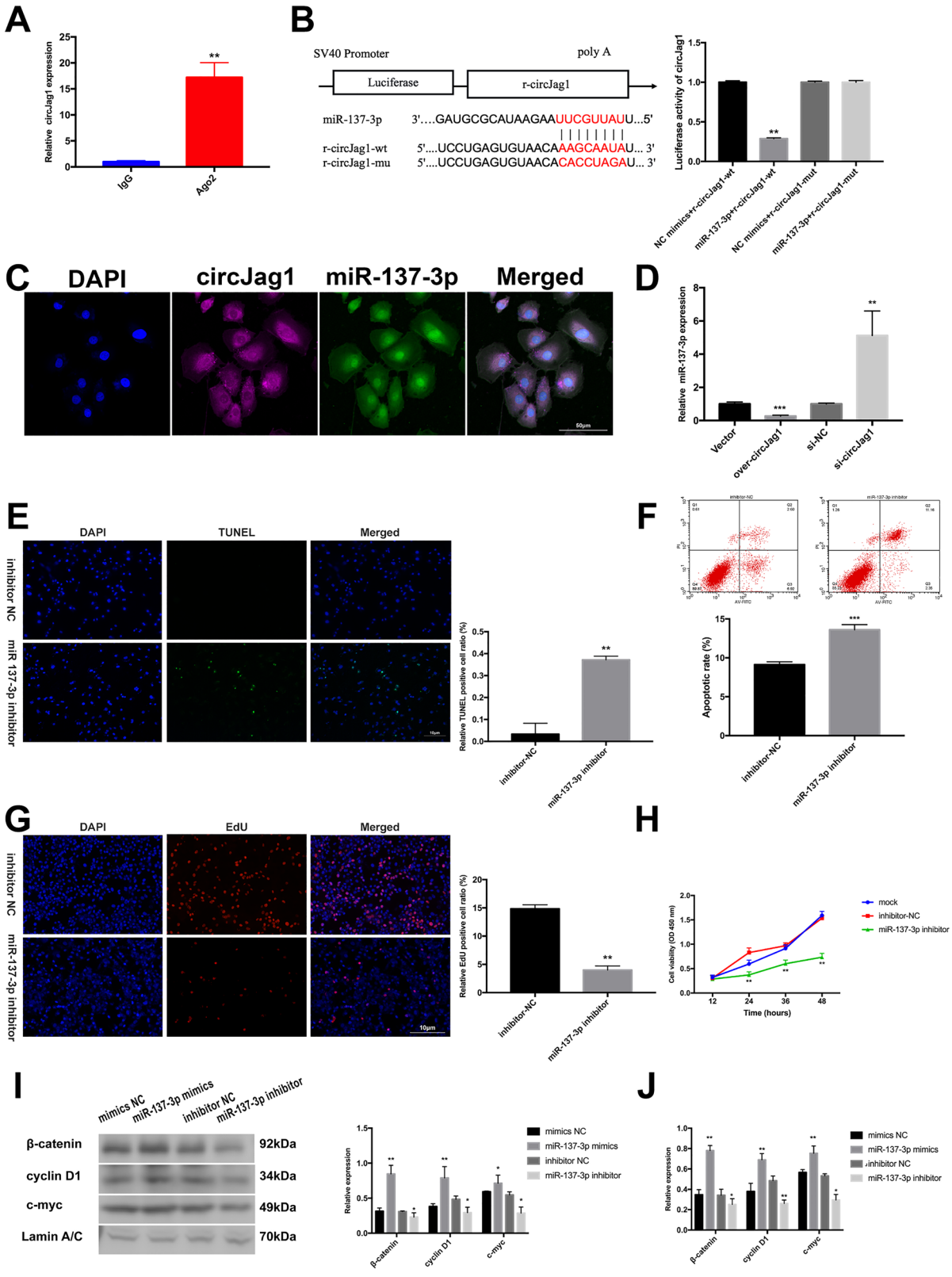
A
Relative circJag1 expression
IgG
Ago2
B
SV40 Promoter
poly A
Luciferase
r-circJag1
miR-137-3p 3'....GAUGCGCAUAAGAAUUCGUUAUU...5'
r-circJag1-wt 5'....UCCUGAGUGUAACAAAGCAAUAU... 3'
r-circJag1-mu 5'....UCCUGAGUGUAACACACCUAGAU... 3'
Luciferase activity of circJag1
NC mimics+r-circJag1-wt
miR-137-3p+r-circJag1-wt
NC mimics+r-circJag1-mut
miR-137-3p+r-circJag1-mut
C
DAPI
circJag1
miR-137-3p
Merged
D
Relative miR-137-3p expression
Vector
over-circJag1
si-NC
si-circJag1
E
DAPI
TUNEL
Merged
inhibitor NC
miR 137-3p inhibitor
Relative TUNEL positive cell ratio (%)
inhibitor-NC
miR-137-3p inhibitor
F
Apoptotic rate (%)
inhibitor-NC
miR-137-3p inhibitor
G
DAPI
EdU
Merged
inhibitor NC
miR-137-3p inhibitor
Relative EdU positive cell ratio (%)
inhibitor-NC
miR-137-3p inhibitor
H
Cell viability (OD 450 nm)
Time (hours)
mock
inhibitor-NC
miR-137-3p inhibitor
I
mimics NC
miR-137-3p mimics
inhibitor NC
miR-137-3p inhibitor
β-catenin
cyclin D1
c-myc
Lamin A/C
92kDa
34kDa
49kDa
70kDa
Relative expression
J
Relative expression

◂**Fig. 3** CircJag1 serves as a sponge for miR-137-3p. **A** Total RNA was extracted from IEC-6 and immunoprecipitated using Ago2 or IgG antibody. CircJag1 amount in the immunoprecipitate was detected by qRT-PCR. **B** Dual-luciferase reporter experiment validating the direct target relationship of circJag1 and miR-137-3p. **C** FISH images showing the colocalization of circJag1 and miR-137-3p in IEC-6. **D** qRT-PCR was used to detect the relative expression levels of miR-137-3p after transfection si-circJag1/si-NC/over-circJag1/vector in IEC-6. U6 was used as an internal control. **E, F** TUNEL and flow cytometry with FITC-Annexin V/PI gating were used to detect apoptosis in IEC-6 after transfection miR-137-3p inhibitor/inhibitor NC. Q2 and Q3 represent the percentage of late and early apoptotic cells in quadrants, respectively. **G, H** EdU and CCK-8 assays were used to detect the viability of IEC-6 after transfection miR-137-3p inhibitor/inhibitor NC. **I** Western blotting was used to detect the protein expression levels of β-catenin, Cyclin D1, and C-myc in nuclear protein after transfection miR-137-3p mimics/mimics-NC/miR-137-3p inhibitor/inhibitor NC. **J** qRT-PCR was used to detect the relative expression levels of β-catenin, Cyclin D1, and C-myc in nuclear RNA after transfection miR-137-3p mimics/mimics-NC/miR-137-3p inhibitor/inhibitor NC. U6 was used as an internal control. $^{*}p < 0.05$; $^{**}p < 0.01$; $^{***}p < 0.001$

These results support our hypothesis that circJag1 serves as a miR-137-3p sponge. Transfection with an miR-137-3p inhibitor increased the rate of apoptosis (Fig. 3E, F) and decreased cell viability and proliferation (Fig. 3G, H). qRT-PCR and Western blotting showed that β-catenin, C-myc, and Cyclin D1 expression decreased/increased significantly in nuclear after treatment with miR-137-3p inhibitor/mimics (Fig. 3I, J).

Deduction of miR-137-3p upregulates Sox9 and inhibits intracellular β-catenin

After co-transfection with a miR-137-3p mimic and the wild-type/mutated 3′-UTR of *Sox9*, the luciferase reporter assay indicated that miR-137-3p could remarkably and specifically inhibit the transcription of Sox9 (Fig. 4A). Transfection with the miR-137-3p mimics/significantly inhibited/promoted the expression of Sox9 (Fig. 4B, C). Transfection with the Sox9 overexpression plasmid reduces β-catenin, C-myc, and Cyclin D1 expression (Fig. 4D), inhibits proliferation, and promotes apoptosis (Fig. 4E, F). These effects were attenuated by treatment with a miR-137-3p mimic (apoptosis rate (%): over-NC + mimics-NC, 23.76±2.87; over-Sox9+mimics-NC, 32.70±2.57; over-Sox9+miR-137-3p mimics, 25.35±2.50; over-NC+miR-137-3p mimics, 16.32±2.87) (Fig. 4D, F). The above results indicate that there are direct binding sites between Sox9 and miR-137-3p, and there is a direct regulatory effect between them in IEC-6 cells. IF showed that Sox9 overexpression/miR-137-3p silencing resulted in the downregulation of nuclear β-catenin (Fig. 4G).

Spatiotemporal co-expression of circJag1/miR-137-3p/Sox9

In order to clearly and dynamically observe morphological changes of cloacal area development in rat embryos at critical time points, immunohistochemical staining was used to evaluate the spatiotemporal expression patterns of Sox9. We found that the positive signals of Sox9 were stronger in ARM group compared with the normal group (Fig. 5A, B).

In ARM group, on GD14, the URS located in high position of cloaca and far away from CM. Sox9-immunopositive signals were abundant in the hindgut and URS (Fig. 5Aa1, b1). On GD15, the URS and CM remained unfused. Sox9-immunopositive signals could be extensively observed on fistula and hindgut epithelium (Fig. 5Aa2, b2). On GD16, the rectal terminus could not connect with outside. Sox9-positive cells could be found in the fistula and rectal epithelium (Fig. 5Aa3, b3). In normal group, on GD14, it is easy to observe that URS almost fused to CM, and the relative frequencies of Sox9-positive signals were faint in that of place (Fig. 5Ac1, d1). On GD15, the URS epithelium and the dorsal CM fusion together, and the URS and anal membrane (AM) fused tissue exhibited faint Sox9 expression (Fig. 5Ac2, d2). On GD16, rupture of the AM was clearly observed, as well as rectum could be in contact with the external environment. Sox9-positive cells could be found in the anorectal epithelium (Fig. 5Ac3, d3).

Moreover, FISH was used to investigate the spatial and temporal expression patterns of circJag1 and miR-137-3p. The FISH results for circJag1-positive cells (pink) and miR-137-3p-positive cells (green) and IF results for Sox9-positive cells (red) are summarized in Fig. 6. On GD14, markedly higher number of circJag1- and Sox9-positive cells in the hindgut and URS could be observed in the ARM group exceeding that in the normal group (Fig. 6b1, b4, d1, and d4). Moreover, miR-137-3p-positive cells were less frequent in ARM hindgut (Fig. 6c1, c4). On GD15, circJag1 and Sox9 levels were significantly

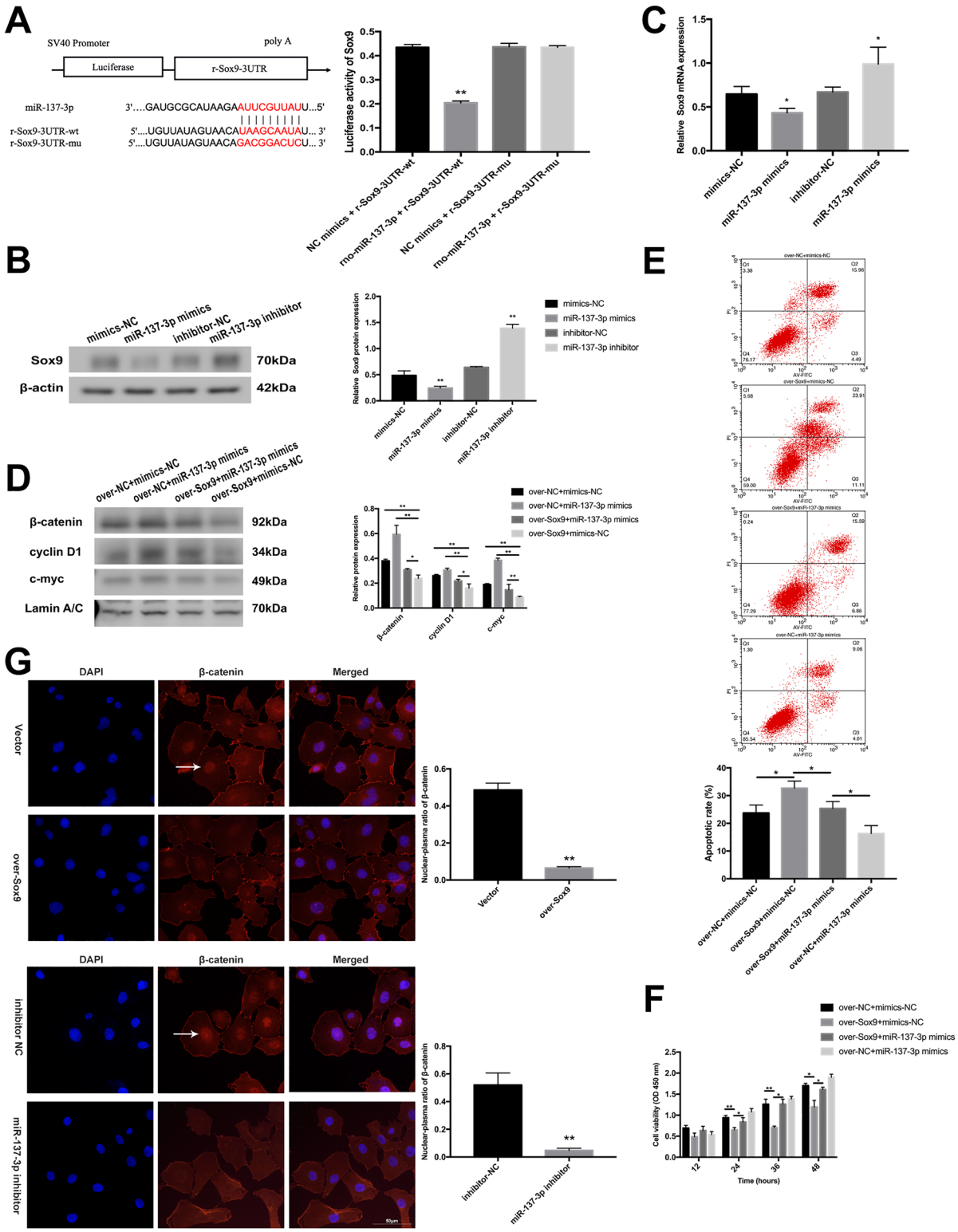
A
SV40 Promoter
poly A
Luciferase
r-Sox9-3UTR
miR-137-3p
3'….GAUGCGCAUAAGAAUUCGUUAUU...5'
r-Sox9-3UTR-wt
5'....UGUUAUAGUAACAUAAGCAAUAU... 3'
r-Sox9-3UTR-mu
5'....UGUUAUAGUAACAGACGGACUCU... 3'
Luciferase activity of Sox9
NC mimics + r-Sox9-3UTR-wt
rno-miR-137-3p + r-Sox9-3UTR-wt
NC mimics + r-Sox9-3UTR-mu
rno-miR-137-3p + r-Sox9-3UTR-mu
C
Relative Sox9 mRNA expression
mimics-NC
miR-137-3p mimics
inhibitor-NC
miR-137-3p mimics
B
mimics-NC
miR-137-3p mimics
inhibitor-NC
miR-137-3p inhibitor
Sox9
β-actin
70kDa
42kDa
Relative Sox9 protein expression
mimics-NC
miR-137-3p mimics
inhibitor-NC
miR-137-3p inhibitor
D
over-NC+mimics-NC
over-NC+miR-137-3p mimics
over-Sox9+miR-137-3p mimics
over-Sox9+mimics-NC
β-catenin
cyclin D1
c-myc
Lamin A/C
92kDa
34kDa
49kDa
70kDa
Relative protein expression
β-catenin
cyclin D1
c-myc
E
over-NC+mimics-NC
over-Sox9+mimics-NC
over-Sox9+miR-137-3p mimics
over-NC+miR-137-3p mimics
Apoptotic rate (%)
over-NC+mimics-NC
over-Sox9+mimics-NC
over-Sox9+miR-137-3p mimics
over-NC+miR-137-3p mimics
G
DAPI
β-catenin
Merged
Vector
over-Sox9
Nuclear-plasma ratio of β-catenin
Vector
over-Sox9
inhibitor NC
miR-137-3p inhibitor
50μm
F
over-NC+mimics-NC
over-Sox9+mimics-NC
over-Sox9+miR-137-3p mimics
over-NC+miR-137-3p mimics
Cell viability (OD 450 nm)
Time (hours)

◂**Fig. 4** miR-137-3p directly targets Sox9. **A** Dual-luciferase reporter experiment validating the direct target relationship of Sox9 and miR-137-3p. **B** Western blotting was used to detect the protein expression levels of Sox9 after transfection miR-137-3p mimics/mimics-NC/miR-137-3p inhibitor/inhibitor NC. **C** qRT-PCR was used to detect the relative mRNA expression levels of Sox9 after transfection miR-137-3p mimics/mimics-NC/miR-137-3p inhibitor/inhibitor NC. β-Actin was used as an internal control. **D** Expression of β-catenin, Cyclin D1, and C-myc in nuclear protein was detected in IEC-6 transfected with over-Sox9, miR-137-3p mimics, or miR-137-3p mimics together with Sox9 plasmid. **E** Flow cytometry with FITC-Annexin V/PI gating was used to detect apoptosis in IEC-6 after transfection over-Sox9, miR-137-3p mimics, or miR-137-3p mimics together with Sox9 plasmid. Q2 and Q3 represent the percentage of late and early apoptotic cells in quadrants, respectively. **F** CCK-8 assays were used to detect the viability of IEC-6 transfected with over-Sox9, miR-137-3p mimics, or miR-137-3p mimics together with Sox9 plasmid. **G** Immunofluorescence was used to detect the effect on β-catenin expression after transfection over-Sox9/vector/miR-137-3p inhibitor/inhibitor NC in IEC-6.The white arrow points to the nuclear positive β-catenin. *$p < 0.05$; **$p < 0.01$

higher in the URS of ARM group, and the AM and URS showed circJag1 and Sox9 signals in the normal group (Fig. 6b2, b5, d2, and d5). The number of circJag1- and Sox9-positive cells were similar. miR-137-3p showed faint expression in the ARM group (Fig. 6c2, c5). Merged images show that their signals overlapped in the fistula and hindgut epithelium (Fig. 6e2, e5). On GD16, circJag1- and Sox9-positive cells were detected in the anorectal epithelium in the normal group (Fig. 6b6, d6). In the ARM group, circJag1- and Sox9-positive cells were abundant in the fistula and terminal rectum, with significant overlap (Fig. 6b3, d3). Positive signals of miR-137-3p were more common in the normal group (Fig. 6c3, c6).

CircJag1 promotes apoptosis and inhibits proliferation through the miR-137-3p/Sox9 axis

The miR-137-3p overexpression remarkably attenuated the circJag1-caused upregulation of Sox9 and downregulation of β-catenin, C-myc, and Cyclin D1 (Fig. 7A, B). The rate of apoptosis was significantly higher in circJag1-overexpressing IECs than in wild-type IECs, and this increase was attenuated by the overexpression of miR-137-3p (apoptosis rate (%): over-NC + mimics-NC, 18.21±2.39; over-circJag1+mimics-NC, 27.02±2.45; over-circJag1+miR-137-3p mimics, 21.07±2.24; over-NC+miR-137-3p mimics, 15.19±0.77) (Fig. 7C, D). To demonstrate the direct interaction between circJag1 and miR-137-3p, we overexpressed miR-137-3p (20, 50, and 100 nM) in IECs after the overexpression of circJag1 (Fig. 7E). This result demonstrated that the effect of miR-137-3p suppressed circJag1-induced Sox9 expression increased in a concentration-dependent manner. These results indicated that circJag1 promotes apoptosis and inhibits proliferation via the miR-137-3p/Sox9 axis.

Apoptotic effect of circJag1 is abolished by the loss of Sox9

CircJag1 overexpression remarkably causes the upregulation of Sox9 together with downregulation of nuclear β-catenin and promoted apoptosis in IECs. Three siRNAs of Sox9 was transfected separately, and the knockout efficiency of si-3 was 74%, which was the most efficient (Fig. S1B). Thus, to silence Sox9, si-3 of it was used in following experiments. We silenced Sox9, followed by transfection with the circJag1 overexpression plasmid/miR-137-3p inhibitor and did not observe an increase in apoptosis or a reduction in proliferation in IECs (Fig. 7F, G). The results mentioned above demonstrated the circJag1/miR-137-3p/Sox9 regulatory axis play an essential role in the regulation of apoptosis together with phenotypic transformation, as well as excess of circJag1 results in more severe epithelial apoptosis.

Discussion

In recent years, researches have evinced circRNAs were important in embryogenesis, skeletal muscle development, neuronal development, osteogenic differentiation, the reproductive system, and germ cell development (Di Agostino et al. 2020; Lee et al. 2019). However, reports on circRNAs during hindgut development are limited. Based on high-throughput sequencing data and an interaction network (Li et al. 2021b), a novel circRNA (circJag1) was identified, and it was significantly upregulated in the hindgut of ARM rat embryos treated with ETU. It is traditionally thought that the failure of the fusion between the URS and CM during the key period (GD14–GD16) for anorectal formation leads to the failure of anorectal separation from the urethra. There is still a normal tube between the urethra and rectum that can be a reason for persistent cloaca or rectourethral fistula

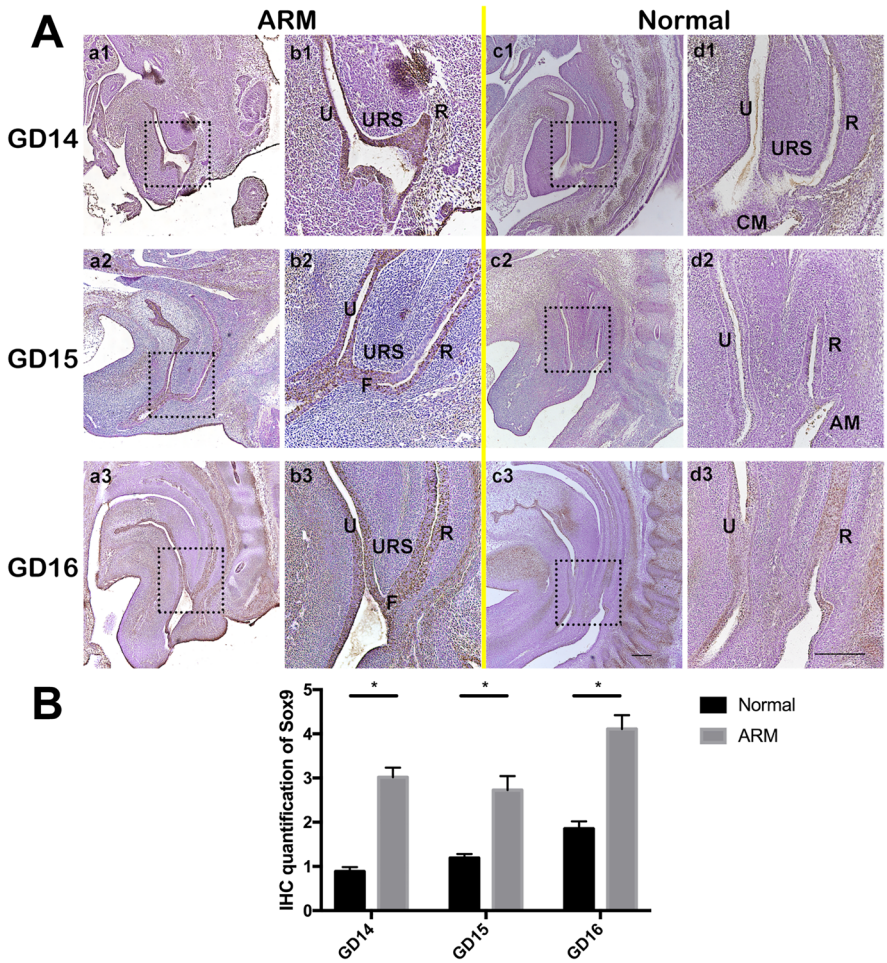

Fig. 5 Immunohistochemical staining of Sox9 in the normal and ARM groups from GD14 to GD16. **A** Black rectangles in **a**, **c** are displayed at higher magnification in **b**, **d**. **B** Quantification of positive signals in IHC. GD, gestational day; U, urethra; R, rectum; URS, urorectal septum; CM, cloacal membrane; F, fistula; AM, anal membrane. Scale bar, 100 μm.*$p < 0.05$

(ARM type) (Qi et al. 2000a; Bai et al. 2004). Our FISH results revealed that there were strong circJag1-positive cell expression on the epithelial cells of the unfused parts in ARM group. qRT-PCR analysis confirmed ARM is associated with higher circJag1 expression during GD14 and GD15. These findings indicated that circJag1 expression undergoes a spatial and temporal imbalance during the development of the anorectum and that it may play a central regulatory role in anorectal abnormalities.

CircRNAs exert biological effects through various mechanisms, e.g., by interacting with RNA polymerase II to regulate transcription; substituting RNA-binding proteins for mRNA splicing patterns; ribosomal translation; and encoding proteins (Ebbesen et al. 2016). Many studies have concentrated on the function of circRNAs as competing endogenous RNA, acting as sponges to suppress miRNAs, and ultimately disturb the conventional mRNAs expression (Hansen et al. 2013). More and more studies have confirmed that circRNAs could regulate post-transcriptional function and often attenuate the repressing influences of miRNAs on their targets (Guil and Esteller 2015). Our results have shown that, circJag1 expression is mainly in the cytoplasm of ICEs, and holds conserved binding sites with miR-137-3p at the same time, which was verified through FISH, dual-luciferase reporter assays, and RNA immunoprecipitation. Overexpression of circJag1 significantly decreased miR-137-3p levels, whereas its absence significantly upregulated miR-137-3p expression. These results verified that, among circJag1 and miR-137-3p had a direct targeted regulatory relationship. Besides, through targeting to the 3′-UTR sequence of Sox9, miR-137-3p could directly inhibits it expression. Notably, overexpression of miR-137-3p could abolish Sox9-mediated epithelial apoptosis. Thus, the isolation effect

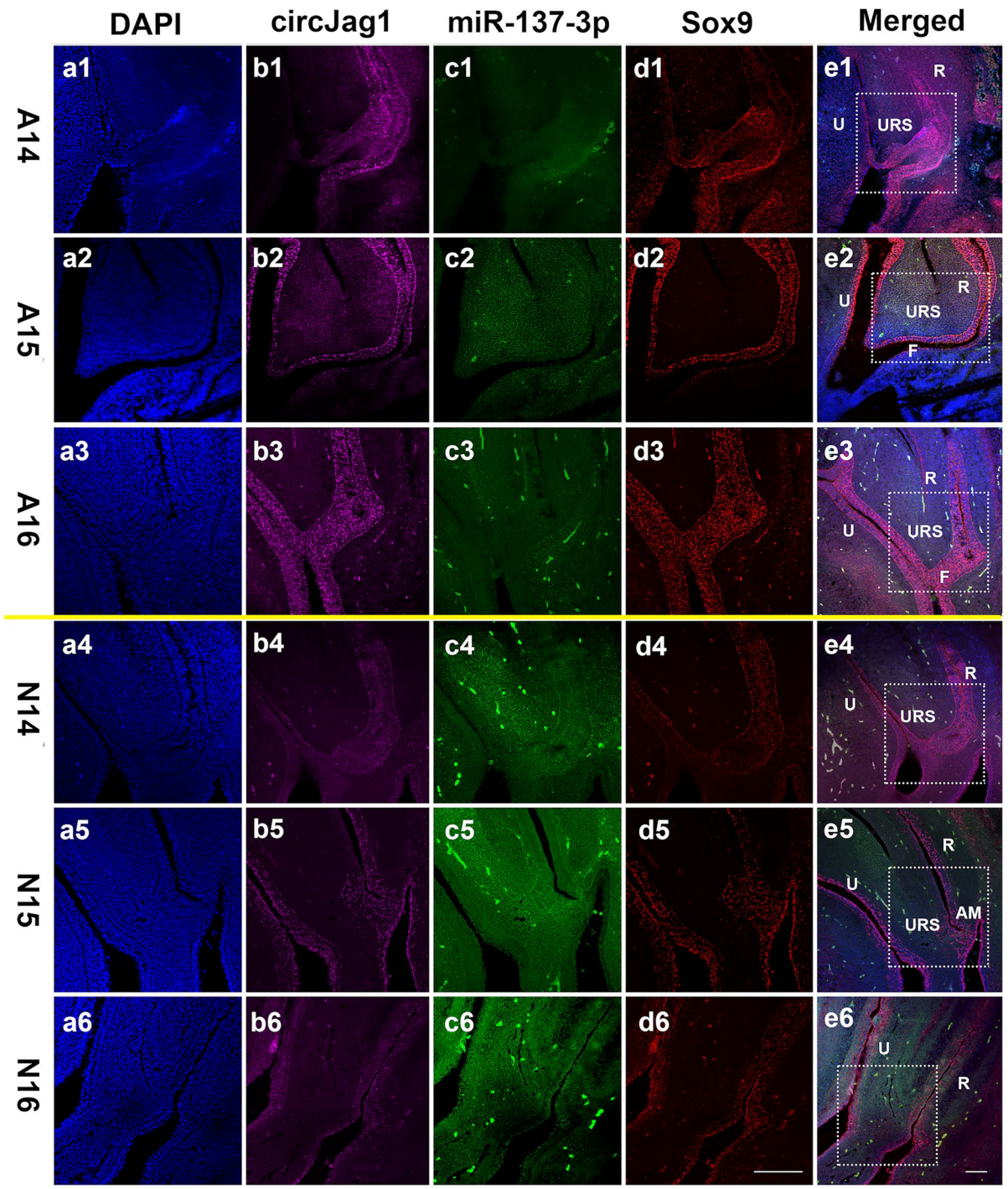

Fig. 6 FISH staining of circJag1 and miR-137-3p together with IF staining of Sox9 in the N and A groups from GD14 to GD16. **a** DAPI (blue); **b** circJag1 (pink); **c** miR-137-3p (green); **d** Sox9 (red); **e** merged images. White rectangles in **e** are displayed at higher magnification in **a**–**d**. N, normal group; A, ARM group; GD, gestational day; U, urethra; R, rectum; URS, urorectal septum; F, fistula; AM, anal membrane. Scale bar, 100 μm

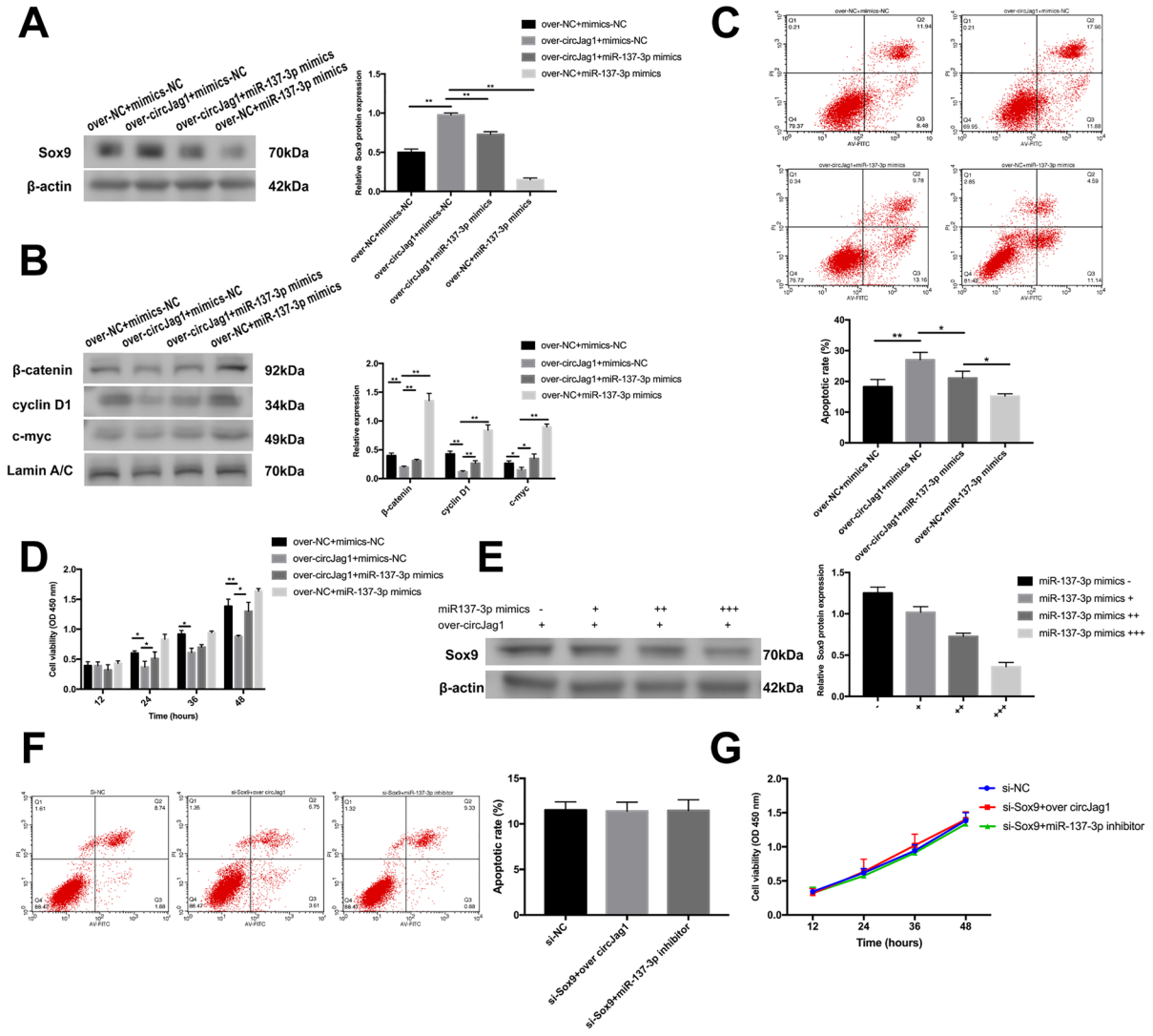

Fig. 7 CircJag1 promotes apoptosis and inhibits proliferation via the miR-137-3p/Sox9 axis. **A**, **B** Expression of Sox9 in total protein and β-catenin, Cyclin D1, and C-myc in nuclear protein was detected in IEC-6 transfected with over-circJag1, miR-137-3p mimics, or miR-137-3p mimics together with over-circJag1. **C** Flow cytometry with FITC-Annexin V/PI gating was used to detect apoptosis in IEC-6 after transfection over-circJag1, miR-137-3p mimics, or miR-137-3p mimics together with over-circJag1. Q2 and Q3 represent the percentage of late and early apoptotic cells in quadrants, respectively. **D** CCK-8 was used to detect the viability of IEC-6 after transfection over-circJag1, miR-137-3p mimics, or miR-137-3p mimics together with over-circJag1. **E** Transfected miR-137-3p mimics (20, 50, and 100 nM) in IECs after the overexpression of circJag1; Western blotting results showed that miR-137-3p inhibited circJag1-induced Sox9 expression increased in a concentration-dependent manner. **F** Apoptotic effect of circJag1 is abolished by the loss of Sox9. Apoptosis assay detected by flow cytometry with FITC-Annexin V/PI gating was used to measure the cell apoptosis of IEC-6 after transfection si-Sox9 together with over-circJag1/miR-137-3p inhibitor. Q2 and Q3 represent the percentage of late and early apoptotic cells in quadrants, respectively. **G** CCK-8 assay was used to measure the cell viability of IEC-6 after co-transfection si-Sox9 together with over-circJag1/miR-137-3p inhibitor. $*p < 0.05$; $**p < 0.01$

of circJag1 on miR-137-3p provides a reverse effect for regulating the effect of miR-137-3p on Sox9. As mentioned above, we reported for the first time the direct regulatory relationships among circJag1, miR-137-3p, and Sox9 and showed that this axis may be an essential part in morphogenesis of anus and rectum.

The delayed development of the tailgut and excessive apoptosis of the epithelial cell in cloaca dorsal wall may be the reason for the dysplasia of the cloaca (Qi et al. 2000b; Li et al. 2021a). Previous studies have confirmed that P53, Bax, and other pro-apoptotic proteins are upregulated during the ARM rat embryos development of hindgut (Li et al. 2021a; Long et al. 2020). According to a series of cell assays, including flow cytometry, TUNEL, CCK8, and EdU assays, we provided the first evidence that circJag1 promotes Sox9 expression by reducing miR-137-3p levels, thereby inducing epithelial apoptosis and inhibiting proliferation.

Apoptosis occurs via many different signaling pathways, among which Wnt/β-catenin as a classical pathway has been widely studied in ARMs. Wnt/β-catenin signal transduction dysregulation can contribute for the ARM phenotypes. Miyagawa et al. (2014) demonstrated that reduced β-catenin expression in the endodermal epithelium by conditional gene knockout results in an ARM phenotype. Ng et al. 2014 found that the Wnt inhibitory factor 1 (*Wif1*) gene, which inhibits Wnt signals, plays a crucial role in cloacal development, providing further evidence for the role of Wnt signaling in the occurrence of ARMs. β-Catenin is a vital molecule in the canonical Wnt pathway. After ligand and receptor binding in the Wnt pathway, the signal transduction leads to the β-catenin aggregated in the cytoplasm. Then, β-catenin enters the nucleus to bind to the TCF/LEF transcription factors that will in turn activate the Cyclin D1and C-myc (effector genes) expression (Kin et al. 2007). Besides, Topol et al. (2009) have investigated the molecular mechanism of Sox9 antagonizing Wnt/β-catenin pathway during chondrocyte differentiation and sought out that the phosphorylation and degradation of β-catenin

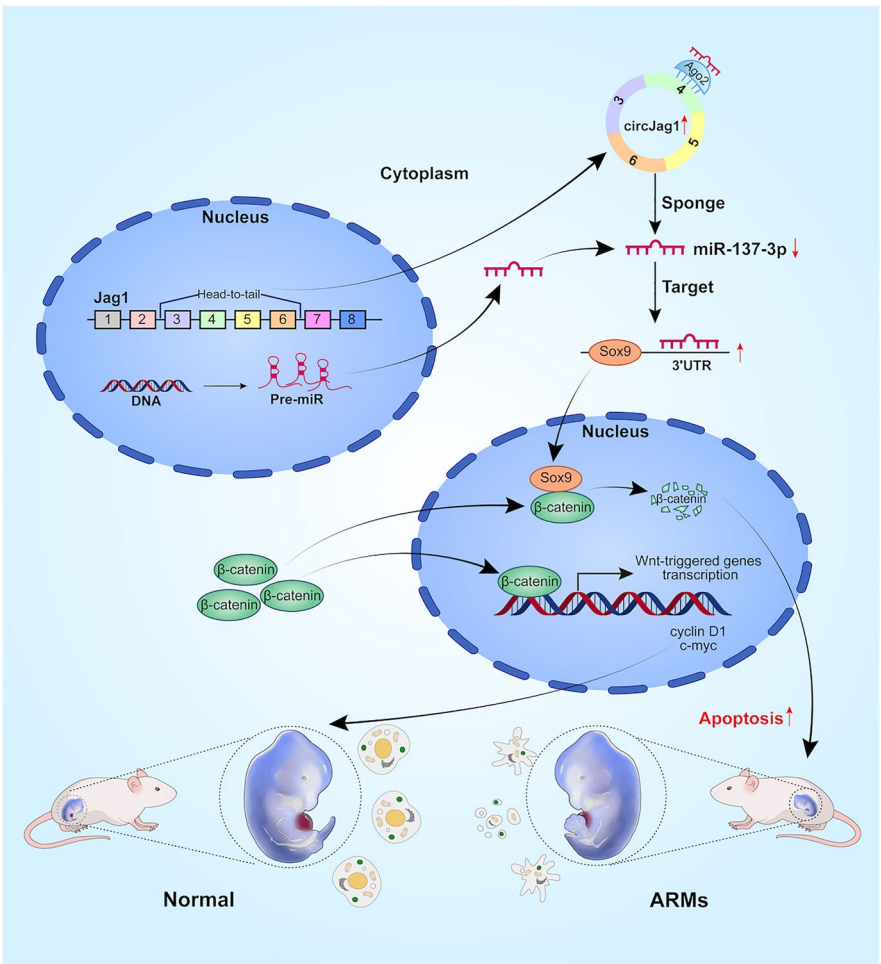

Fig. 8 Proposed model of IEC-6 phenotypic modulation control by circJag1. CircJag1 is generated by the back splicing of exons 3 to 6 of the Jag1 gene. We provide the first study to show that circJag1 performs its potential function as a competing endogenous RNA to sequester miR-137-3p, resulting in activation of miR-137-3p-target Sox9, and then promote degradation of β-catenin and turn off Wnt signaling pathway, thereby resulting in fusion failure of urorectal septum and cloacal membrane by reducing epithelial proliferation and promoting apoptosis, which may lead to anorectal malformations

in the nucleus could be promoted by N-terminus of Sox9. Besides, C-terminus is required to inhibit transcriptional activity of β-catenin without affecting its stability. In this study, we first explored whether circJag1/miR-137-3p/Sox9 had similar potential regulatory effects in intestinal epithelial cells on canonical Wnt/β-catenin signaling pathway. Not only β-catenin protein expression was evaluated, but also the intracellular location after up- and downregulation of circJag1/miR-137-3p/Sox9 were detected. Overall, upregulation of circJag1/Sox9 and downregulation of miR-137-3p were found to lead to β-catenin degradation in the nucleus, thereby reducing its downstream target genes expression including C-myc and Cyclin D1. Hence, based on the molecular biological functions of Wnt/β-catenin, we believe that circJag1/miR-137-3p/Sox9 could exercise a momentous regulatory function in the occurrence and development of ARMs by influencing the epithelial cells apoptosis and proliferation through Wnt/β-catenin pathway (Fig. 8).

Nevertheless, there are several limitations in the study. Although our experimental results support that circJag1 can regulate apoptosis and proliferation through the axis of miR-137-3p/Sox9, in vivo experiments to explore their effects on the phenotype of ARMs are still lacking. In addition, for a further understanding of the character of circJag1 in ARMs, more effort and investigations will be needed. Amniotic fluid and blood samples from the birth cohort should be used in future relevant tests to deeper detect whether circJag1 can be added to a prenatal diagnosis marker or therapeutic target of ARMs.

In conclusion, our results demonstrated that circJag1 is upregulated and exhibits spatiotemporal dysregulated expression during hindgut development in rat embryos with ARMs. Moreover, circJag1 serves as a miR-137-3p sponge and contributes to ARMs via Sox9-mediated epithelial apoptosis. The overexpression of circJag1/Sox9 and repression of miR-137-3p could turn off the Wnt/β-catenin signaling. Taken together, the new mechanism about circJag1 in the epigenetic regulation of Sox9 was revealed. Furthermore, all of the results reveal that circJag1 may have a vital function in anorectal morphogenesis. Notably, the circJag1/miR-137-3p/Sox9 axis may represent a potential therapeutic target for ARMs.

Author contribution S. Y. L. and Y. Z. B. designed the experiments. S. Y. L. performed the experiments and wrote the manuscript. C. Y. W. and X. G. W. analyzed the data. X. B. T and Y. Z. B. performed development of review and revision of the paper. Z. W. Y. provided technical and material support.

Funding The present work was supported by the National Natural Science Foundation of China (grant number 81770511, 82070530 and 82170530), the Liaoning Revitalization Talents Program (grant number XLYC1908008), and the Outstanding Scientific Fund of Shengjing Hospital (grant number ME56).

Data availability Data available on request from the authors. The original data of RNA-Seq are available in the Gene Expression Omnibus database (GSE159306).

Code availability Not applicable.

Declarations

Ethics approval Not applicable

Consent to participate Not applicable

Consent for publication Not applicable

Competing interests The authors declare no competing interests.

References

Akiyama H, Lyons JP, Mori-Akiyama Y, Yang X, Zhang R, Zhang Z, et al. Interactions between Sox9 and beta-catenin control chondrocyte differentiation. Genes Dev. 2004;18(9):1072–87. https://doi.org/10.1101/gad.1171104.

Anguissola S, McCormack WJ, Morrin MA, Higgins WJ, Fox DM, Worrall DM. Pigment epithelium-derived factor (PEDF) interacts with transportin SR2, and active nuclear import is facilitated by a novel nuclear localization motif. PLoS One. 2011;6(10):e26234. https://doi.org/10.1371/journal.pone.0026234.

Bai Y, Yuan Z, Wang W, Zhao Y, Wang H, Wang W. Quality of life for children with fecal incontinence after surgically corrected anorectal malformation. J Pediatr Surg. 2000;35(3):462–4. https://doi.org/10.1016/s0022-3468(00)90215-x.

Bai Y, Chen H, Yuan ZW, Wang W. Normal and abnormal embryonic development of the anorectum in rats. J Pediatr Surg. 2004;39(4):587–90. https://doi.org/10.1016/j.jpedsurg.2003.12.002.

Bastide P, Darido C, Pannequin J, Kist R, Robine S, Marty-Double C, et al. Sox9 regulates cell proliferation and is required for Paneth cell differentiation in the intestinal epithelium. J Cell Biol. 2007;178(4):635–48. https://doi.org/10.1083/jcb.200704152.

Chatzeli L, Gaete M, Tucker AS. Fgf10 and Sox9 are essential for the establishment of distal progenitor cells

during mouse salivary gland development. Development. 2017;144(12):2294–305. https://doi.org/10.1242/dev.146019.

Di Agostino S, Riccioli A, De Cesaris P, Fontemaggi G, Blandino G, Filippini A, et al. Circular RNAs in embryogenesis and cell differentiation with a focus on cancer development. Front Cell. Dev Biol. 2020;8:389. https://doi.org/10.3389/fcell.2020.00389.

Ebbesen KK, Kjems J, Hansen TB. Circular RNAs: identification, biogenesis and function. Biochim Biophys Acta. 2016;1859(1):163–8. https://doi.org/10.1016/j.bbagrm.2015.07.007.

Falcone RA Jr, Levitt MA, Peña A, Bates M. Increased heritability of certain types of anorectal malformations. J Pediatr Surg. 2007;42(1):124–7; discussion 127-8. https://doi.org/10.1016/j.jpedsurg.2006.09.012.

Formeister EJ, Sionas AL, Lorance DK, Barkley CL, Lee GH, Magness ST. Distinct SOX9 levels differentially mark stem/progenitor populations and enteroendocrine cells of the small intestine epithelium. Am J Physiol Gastrointest Liver Physiol. 2009;296(5):G1108–18. https://doi.org/10.1152/ajpgi.00004.2009.

Grano C, Bucci S, Aminoff D, Lucidi F, Violani C. Quality of life in children and adolescents with anorectal malformation. Pediatr Surg Int. 2013;29(9):925–30. https://doi.org/10.1007/s00383-013-3359-8.

Guil S, Esteller M. RNA-RNA interactions in gene regulation: the coding and noncoding players. Trends Biochem Sci. 2015;40(5):248–56. https://doi.org/10.1016/j.tibs.2015.03.001.

Haegel H, Larue L, Ohsugi M, Fedorov L, Herrenknecht K, Kemler R. Lack of beta-catenin affects mouse development at gastrulation. Development. 1995;121(11):3529–37. https://doi.org/10.1242/dev.121.11.3529.

Hansen TB, Jensen TI, Clausen BH, Bramsen JB, Finsen B, Damgaard CK, et al. Natural RNA circles function as efficient microRNA sponges. Nature. 2013;495(7441):384–8. https://doi.org/10.1038/nature11993.

Kamachi Y, Kondoh H. Sox proteins: regulators of cell fate specification and differentiation. Development. 2013;140(20):4129–44. https://doi.org/10.1242/dev.091793.

Khanna K, Sharma S, Pabalan N, Singh N, Gupta DK. A review of genetic factors contributing to the etiopathogenesis of anorectal malformations. Pediatr Surg Int. 2018;34(1):9–20. https://doi.org/10.1007/s00383-017-4204-2.

Kim BM, Mao J, Taketo MM, Shivdasani RA. Phases of canonical Wnt signaling during the development of mouse intestinal epithelium. Gastroenterology. 2007;133(2):529–38. https://doi.org/10.1053/j.gastro.2007.04.072.

Kluth D. Embryology of anorectal malformations. Semin Pediatr Surg. 2010;19:201–8.

Lasda E, Parker R. Circular RNAs: diversity of form and function. RNA. 2014;20(12):1829–42. https://doi.org/10.1261/rna.047126.114.

Lee E, Elhassan S, Lim G, Kok WH, Tan SW, Leong EN, et al. The roles of circular RNAs in human development and diseases. Biomed Pharmacother. 2019;111:198–208. https://doi.org/10.1016/j.biopha.2018.12.052.

Li SY, Wang CY, Zhao JJ, Long CY, Xiao YX, Tang XB, et al. Upregulation of PPPDE1 contributes to anorectal malformations via the mitochondrial apoptosis pathway during hindgut development in rats. Exp Cell Res. 2021a;402(2):112574. https://doi.org/10.1016/j.yexcr.2021.112574.

Li SY, Wang CY, Xiao YX, Tang XB, Yuan ZW, Bai YZ. RNA-Seq profiling of circular RNAs during development of hindgut in rat embryos with ethylenethiourea-induced anorectal malformations. Front Genet. 2021b;12:605015. https://doi.org/10.3389/fgene.2021.605015.

Liu YR, Ba F, Cheng LJ, Li X, Zhang SW, Zhang SC. Efficacy of Sox10 promoter methylation in the diagnosis of intestinal neuronal dysplasia from the peripheral blood. Clin Transl Gastroenterol. 2019;10(12):e00093. https://doi.org/10.14309/ctg.0000000000000093.

Long C, Xiao Y, Li S, Tang X, Yuan Z, Bai Y. Involvement of proliferative and apoptotic factors in the development of hindgut in rat fetuses with ethylenethiourea-induced anorectal malformations. Acta Histochem. 2020;122(1):151466. https://doi.org/10.1016/j.acthis.2019.151466.

Macedo M, Martins JL, Meyer KF. Evaluation of an experimental model for anorectal anomalies induced by ethylenethiourea. Acta Cir Bras. 2007;22(2):130–6. https://doi.org/10.1590/s0102-86502007000200010.

Mandhan P, Quan QB, Beasley S, Sullivan M. Sonic hedgehog, BMP4, and Hox genes in the development of anorectal malformations in ethylenethiourea-exposed fetal rats. J Pediatr Surg. 2006;41(12):2041–5. https://doi.org/10.1016/j.jpedsurg.2006.08.035.

Misir S, Wu N, Yang BB. Specific expression and functions of circular RNAs. Cell Death Differ. 2022;29(3):481–91. https://doi.org/10.1038/s41418-022-00948-7.

Miyagawa S, Harada M, Matsumaru D, Tanaka K, Inoue C, Nakahara C, et al. Disruption of the temporally regulated cloaca endodermal β-catenin signaling causes anorectal malformations. Cell Death Differ. 2014;21(6):990–7. https://doi.org/10.1038/cdd.2014.21.

Ng RC, Matsumaru D, Ho AS, Garcia-Barceló MM, Yuan ZW, Smith D, et al. Dysregulation of Wnt inhibitory factor 1 (Wif1) expression resulted in aberrant Wnt-β-catenin signaling and cell death of the cloaca endoderm, and anorectal malformations. Cell Death Differ. 2014;21(6):978–89. https://doi.org/10.1038/cdd.2014.20.

Qi BQ, Williams A, Beasley S, Frizelle F. Clarification of the process of separation of the cloaca into rectum and urogenital sinus in the rat embryo. J Pediatr Surg. 2000a;35(12):1810–6. https://doi.org/10.1053/jpsu.2000.19265.

Qi BQ, Beasley SW, Williams AK, Fizelle F. Apoptosis during regression of the tailgut and septation of the cloaca. J Pediatr Surg. 2000b;35(11):1556–61. https://doi.org/10.1053/jpsu.2000.18309.

Qi BQ, Beasley SW, Frizelle FA. Clarification of the processes that lead to anorectal malformations in the ETU-induced rat model of imperforate anus. J Pediatr Surg. 2002;37(9):1305–12. https://doi.org/10.1053/jpsu.2002.34996.

Sasaki C, Yamaguchi K, Akita K. Spatiotemporal distribution of apoptosis during normal cloacal development in mice. Anat Rec A Discov Mol Cell Evol Biol. 2004;279(2):761–7. https://doi.org/10.1002/ar.a.20062.

Schepers GE, Teasdale RD, Koopman P. Twenty pairs of sox: extent, homology, and nomenclature of the mouse

and human sox transcription factor gene families. Dev Cell. 2002;3(2):167–70. https://doi.org/10.1016/s1534-5807(02)00223-x.

Shi Z, Chiang CI, Mistretta TA, Major A, Mori-Akiyama Y. SOX9 directly regulates IGFBP-4 in the intestinal epithelium. Am J Physiol Gastrointest Liver Physiol. 2013;305(1):G74–83. https://doi.org/10.1152/ajpgi.00086.2013.

Song H, Park KH. Regulation and function of SOX9 during cartilage development and regeneration. Semin Cancer Biol. 2020;67(Pt 1):12–23. https://doi.org/10.1016/j.semcancer.2020.04.008.

Tang XB, Zhang T, Wang WL, Yuan ZW, Bai YZ. Temporal and spatial expression of caudal-type homeobox gene-2 during hindgut development in rat embryos with ethylenethiourea-induced anorectal malformations. Cell Tissue Res. 2014;357(1):83–90. https://doi.org/10.1007/s00441-014-1858-0.

Topol L, Chen W, Song H, Day TF, Yang Y. Sox9 inhibits Wnt signaling by promoting beta-catenin phosphorylation in the nucleus. J Biol Chem. 2009;284(5):3323–33. https://doi.org/10.1074/jbc.M808048200.

Wang C, Li L, Cheng W. Anorectal malformation: the etiological factors. Pediatr Surg Int. 2015;31(9):795–804. https://doi.org/10.1007/s00383-015-3685-0.

Wijers CH, van Rooij IA, Marcelis CL, Brunner HG, de Blaauw I, Roeleveld N. Genetic and nongenetic etiology of nonsyndromic anorectal malformations: a systematic review. Birth Defects Res C Embryo Today. 2014;102(4):382–400. https://doi.org/10.1002/bdrc.21068.

Wood RJ, Levitt MA. Anorectal malformations. Clin Colon Rectal Surg. 2018;31(2):61–70. https://doi.org/10.1055/s-0037-1609020.

Zhou J, Ge Y, Hu Y, Rong D, Fu K, Wang H, et al. Circular RNAs as novel rising stars with huge potentials in development and disease. Cancer Biomark. 2018;22(4):597–610. https://doi.org/10.3233/CBM-181296.

Zhou Y, Li C, Wang Z, Tan S, Liu Y, Zhang H, et al. CircRNAs as novel biomarkers and therapeutic targets in renal cell carcinoma. Front Mol Biosci. 2022;9:833079. https://doi.org/10.3389/fmolb.2022.833079.